Self-focusing of a single laser pulse in a photorefractive medium

D. Wolfersberger, N. Fressengeas, J. Maufoy, and G. Kugel
Laboratoire Matériaux Optiques, Photonique et Systèmes, Université de Metz et Supélec, 2 rue Edouard Belin, 57070 Metz Cedex, France

(Received 12 April 2000)

An original experimental and theoretical time-resolved study of a single laser pulse self-focusing in a nonlinear photorefractive medium is reported. The behavior of the self-focusing process is experimentally observed in a photorefractive $Bi_{12}TiO_{20}$ crystal during the 5 ns pulse duration of a doubled Nd:YAG (yttrium aluminum garnet) laser. A theoretical interpretation is provided, based on a simple model of photorefraction on the nanosecond time scale.

PACS number(s): 42.65.Tg, 42.65.Hw, 42.65.Jx, 42.65.Sf

I. INTRODUCTION

Beam self-focusing and self-trapping in photorefractive media are today deeply studied subjects, at least as far as the photorefractive steady state is concerned. Indeed, photorefractive materials are known to allow beam self-focusing [1,2] or defocusing [3], leading to the possible prediction [4] and observation [5] of spatial solitons. These phenomena arise mainly on biasing the photorefractive sample through the application of an electric field [6,7] or by the mere presence of a photovoltaic or photogalvanic [8] effect. Insight into the process of their buildup has also been obtained theoretically [9,10] and experimentally [11]. The outcome of these few time-resolved studies is the knowledge that one may expect significant photorefractive self-focusing at times as short as desired, provided the incident light intensity can be raised enough or the dark or background irradiance can be lowered enough [12].

Although most of the work reported in the literature deals with continuous wave laser beams at low power level, the recent literature reports that self-focusing leading to spatial solitons occurs in photorefractive media under repetitive pulsed illumination [13], in accordance with previously developed theoretical predictions [14].

We have conducted *time-resolved* experiments in order to investigate the temporal behavior of a single pulse self-focusing in photorefractive $Bi_{12}TiO_{20}$ and we have developed a $(1+1)$-dimensional theoretical model to explain our observations.

II. EXPERIMENTAL EVIDENCE OF SELF-FOCUSING

The experimental setup is shown in Fig. 1. The 532 nm output from a potassium triphosphate (KTP) doubled Nd:YAG (yttrium aluminum garnet) laser emitting an energy equal to 17 mJ is strongly attenuated and focused on a 6.4 mm long $Bi_{12}TiO_{20}$ crystal, the light propagation direction being along [110]. The circular 20 μm beam waist is carefully monitored and set on the entrance face of the crystal sample, its peak fluence being around 5 mJ/cm^2 for a 5 ns laser pulse. A strong electric field on the order of a few kV/cm is applied to the $Bi_{12}TiO_{20}$ sample in the $[1\bar{1}0]$ direction, perpendicular to the laser beam.

The beam diameter in the direction parallel to the field is monitored using a real time experimental observation method based on a far field spatial filtering technique. A 1 mm wide vertical slit, in the direction orthogonal to the external applied electric field, is set 140 mm away from the crystal output face: in this configuration, the overall light power passing through the slit and collected by the photodiode can be considered as proportional to the output beam waist. It thus yields an instantaneous time-resolved measurement of the output beam diameter, provided the beam is not bent in the photorefractive propagation medium and thus remains globally centered on the same spot. More details of the measurement method are given in the following as well as in Refs. [10,11].

As a preliminary, before systematic measurements of self-focusing could be undertaken, the requirement that the beam does not bend had to be verified carefully since Aguilar *et al.* [15] have reported transient self-bending due to drift nonlinearity (i.e., applied electric field), although on time scales (seconds) very different from ours. The check was done by imaging the crystal output face on a fast position detector

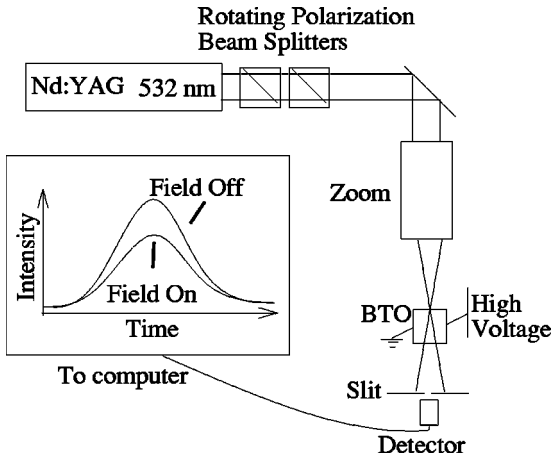

FIG. 1. Experimental setup. The inset gives a typical time-resolved scheme of the light intensity, proportional in real time to the output beam waist, with the electric field off and on. Real measurements are reported in Fig. 2(a).

consisting of two side by side photodiodes several micrometers apart, allowing us to evidence potential bending of the beam during the pulse duration. This technique allowed us to ascertain that, for fluences on the order of 5 mJ/cm^2, waists around 20 μm, and electric fields of a few kV/cm, no significant transient self-bending of a single pulse can be observed in our $Bi_{12}TiO_{20}$ sample. This observation was confirmed by the model developed and presented in the next section: a significant self-bending can only be achieved in simulation with an unrealistic applied electric field of a few MV/cm.

The influence of the polarization of the beam on the entrance face of the crystal and its behavior during propagation have also been studied carefully. $Bi_{12}TiO_{20}$ is a crystal of the sillenite family which exhibits a gyratory power of 11°/mm at 532 nm, giving an overall gyration of 70.4° in our sample. Earlier studies on $Bi_{12}TiO_{20}$ [11,16] have approximated the role of the polarization by prerotating the input polarization plane so as to compensate for half the crystal-induced gyration and thus minimize the maximum angle between the polarization and the electric field directions.

In our case, taking into account the crystal length, this minimum is still 35.2°. Therefore, rather than neglecting the polarization gyration, we chose to conduct our studies with a beam polarized so as to get the strongest self-focusing effect. For that, several measurements were done with various input polarizations. The maximum self-focusing power under applied field was found to occur for an output polarization parallel to the electric field, namely, an input polarization of $-70.4°$.

Once it is ascertained that the beam remains globally centered and the polarization is carefully set, the experimental setup described in Fig. 1 yields a time-resolved measurement of the light intensity passing through the slit proportional in real time to the output beam waist. In order to study the behavior of the self-focusing process during one pulse, the temporal profile of the overall power is then acquired twice, as shown on the inset in Fig. 1 and in more detail in Fig. 2(a): a first time with no electric field in order to set a reference, the $Bi_{12}TiO_{20}$ (BTO) sample being considered linear, and a second time with the proper electric field on, the nonlinearity being activated. Figure 2 shows such typical time resolved measurements in another BTO sample whose length equals 3.17 mm. Figure 2(a) shows that the intensity collected with the electric field on, $I(t)$, is less than that with the field off, $I_d(t)$. When the output beam waist becomes smaller, the diffraction from the output face of the crystal is more important and thus the intensity passing through the slit is less important. As described in [10,11], in our case, the intensity passing through the slit is proportional to the output beam diameter. In other words, the decrease of the intensity is evidence of beam self-focusing. The point to point ratio of these two sets of values $I(t)/I_d(t)$ is a time-resolved result proportional to the output beam waist normalized to the input beam waist. We have called it the *diffraction coefficient* α. The exact value of the diffraction coefficient $\alpha(t)$ can be deduced from the relation $\alpha(t)=\alpha_r I(t)/I_d(t)$, α_r being the diffraction coefficient when no electric field is applied. α_r is evaluated theoretically by considering the propagation of a Gaussian beam in a linear medium. A typical measurement of the temporal evolution of the diffraction coefficient $\alpha(t)$

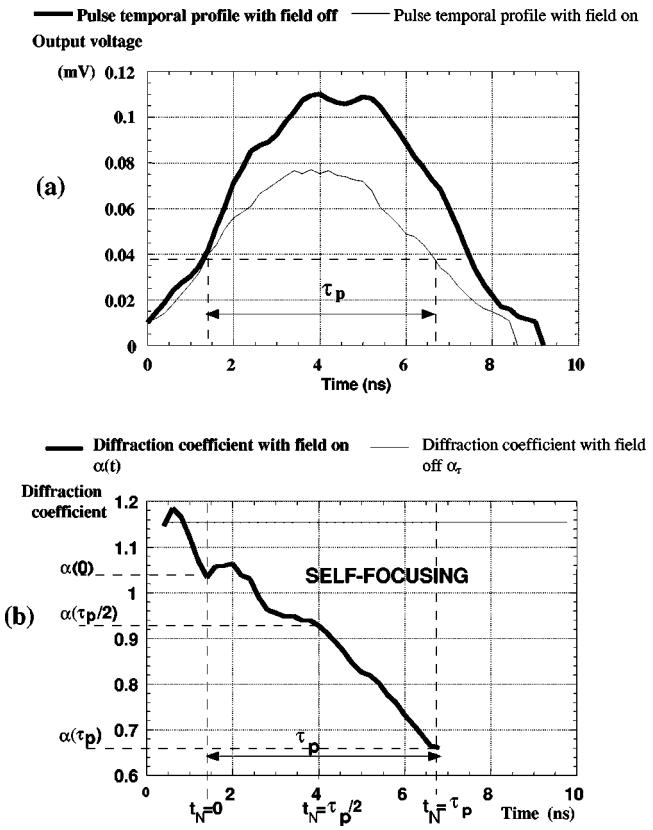

FIG. 2. Typical time-resolved measurements on a $Bi_{12}TiO_{20}$ sample whose length equals 3.17 mm. (a) The pulse temporal profile at the output face of the crystal with field off (thick line) and on (thin line). (b) The corresponding measured diffraction coefficient under applied electric field. $\alpha(t)$ represents the measured diffraction coefficient during one pulse when the crystal is under an external applied electric field; α_r corresponds to the diffraction coefficient when the crystal can be considered as linear (no applied electric field). The pulse half width at half maximum is noted, τ_p, and is around 5 ns. $t_N=0$, $t_N=\tau_p/2$, and $t_N=\tau_p$ represent times corresponding to the beginning, the maximum, and the end of the pulse for analysis.

during one pulse is presented in Fig. 2(b), corresponding to the average of 20 measurements in the same conditions. Owing to measurement noise issues, the measurement time window was centered on the pulse maximum and its width was set to the pulse half width at half maximum τ_p (around 5 ns). We note a decrease of the diffraction coefficient during the pulse, showing self-focusing of the beam when it passes through the crystal. For analyzing the results, we note $t_N=0$, $t_N=\tau_p/2$, and $t_N=\tau_p$, the times corresponding, respectively, to the beginning, the maximum, and the end of the pulse [Fig. 2(a)]. All values of α between $t_N=0$ and $t_N=\tau_p$ are then given as shown in Fig. 2(b).

Figure 3 reports various time dependencies of experimental and theoretical diffraction coefficients as will be detailed in the following. The solid line in Fig. 3 shows one typical measurement of the diffraction coefficient evolution of a light pulse during its duration for an applied field of 6.25 kV/cm, a 5 mJ/cm^2 fluence, and an input beam waist of 20 μm, the diffraction coefficient being measured in the direction parallel to the field (the slit is perpendicular to it).

The particular example shown in Fig. 3 is representative

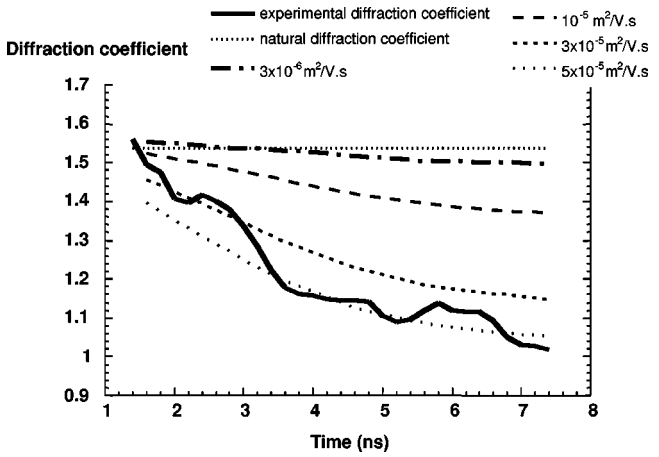

FIG. 3. Diffraction coefficient vs time. The black solid line shows the experimental data whereas the dashed lines show theoretically predicted curves corresponding to mobilities of $\mu = 3\times10^{-2}$ cm^2/V s, $\mu = 0.1$, $\mu = 0.3$, and $\mu = 0.5$ cm^2/V s (from top to bottom). The horizontal dotted line is the rest diffraction coefficient, when the crystal is considered to be linear.

of our global measurement series in the way that it shows a progressive continuous decrease of the diffraction coefficient during the laser pulse. Indeed, in spite of the fact that the beam intensity is less at the end of the pulse than at its maximum, the beam is more self-focused at the end of the time window. As our theoretical analysis points out, this is due to the fact that the self-focusing process stems from a progressive electric field screening at the spot of the beam. This has been observed for all applied electric fields between 0 and 6.25 kV/cm, and for fluences between 1 and 5 mJ/cm^2. The beam was observed to be more self-focused as the fluence or the electric field is increased, as shown in the inset of Fig. 4.

As presented above, these self-focusing features under applied electric field are attributed to the photorefractive properties of $Bi_{12}TiO_{20}$. This assumption is checked in the next section against a simple model of photorefraction in the nanosecond regime.

III. INTERPRETATION

The simplest description of photorefraction is with a model derived from the general set of equations developed by Kukhtarev *et al.* [17]. In the case of illumination by a single powerful nanosecond laser pulse, the thermal generation of charge carriers can be neglected. Furthermore, since we attempt to describe phenomena occurring in $Bi_{12}TiO_{20}$, we will consider, in the Kukhtarev equations, the natural carrier diffusion and the photovoltaic effect to be negligible with respect to the drift transport mechanism due to the applied electric field of a few kV/cm.

Under these assumptions, considering times shorter than the charge carrier recombination time, and reducing the charge transport model to one dimension x, a partial differential equation linking the scalar internal electric field E and the beam intensity I_{em} can be derived:

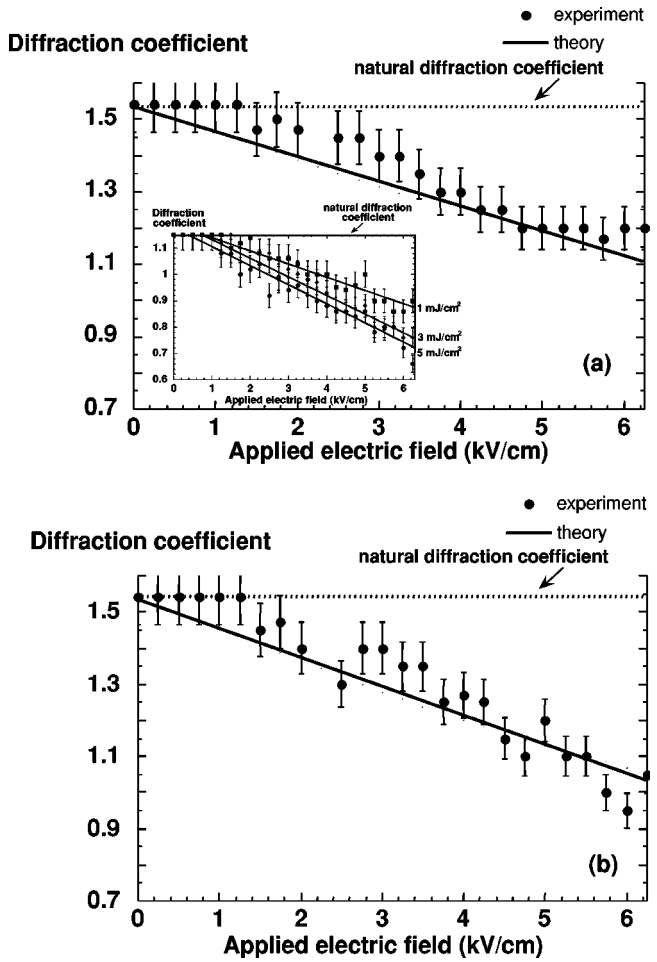

FIG. 4. Diffraction coefficient vs applied electric field. (a) and (b) show the measured diffraction coefficient in the middle and at the end of the time window, the two solid lines showing the corresponding theoretical predictions for $\mu = 0.5$ cm^2/V s. The inset in (a) shows the measured diffraction coefficient in the middle of the time window vs applied electric field for various incident fluences but on another sample of $Bi_{12}TiO_{20}$ of a shorter length, equal to 3.17 mm.

$$\varepsilon_0\varepsilon_r\left(\frac{\partial^2 E}{\partial x\,\partial t}-\mu E\frac{\partial^2 E}{\partial x^2}\right)+e\mu(N_D-N_A)$$
$$\times[1-\exp(-sI_{em}t)]\frac{\partial E}{\partial x}+e\mu s(N_D-N_A)t$$
$$\times\exp(-sI_{em}t)\frac{\partial I_{em}}{\partial x}E=0. \qquad (1)$$

where the internal electric field E and the beam local intensity I_{em} are functions of space and time t. The material-dependent parameters are the photoionization cross section s, the donor and acceptor densities N_D and N_A, the electron mobility μ, and the static dielectric constant ε_r. The standard physical constants are thus defined as e, the elementary charge, and ε_0, the vacuum electric permeability.

Equation (1) can be solved numerically for the electric field **E** provided that a spatial distribution of light intensity I_{em} is input. This latter is obtained by solving the general $(1+1)$-dimensional $[(1+1)\mathrm{D}]$ wave propagation equation

(2) in a medium with a small refractive index variation by using standard beam propagation method (BPM) techniques, k being the wave vector in the medium, n and δn the refractive index and its variation, and $\mathcal{E}$ the wave electric field:

$$\left(\frac{\partial}{\partial z}-\frac{i}{2k}\frac{\partial^2}{\partial x^2}\right)\mathcal{E}=\frac{ik}{n}\delta n\mathcal{E}. \tag{2}$$

We consider in the above equation that the beam propagates along the z direction and is allowed to diffract in only one direction x [$(1+1)$D model]. The beam propagation method consists in dividing the photorefractive crystal along its length (z direction) into different transverse 1D slices (parallel to the x direction) of equal thickness h. Assuming a homogeneous photorefractive medium at the beginning of the laser pulse, the first step in time for the BPM calculation is computed using a homogeneously null index variation δn ($\delta n=0$) and propagating a given input beam (e.g., a Gaussian profile). Solving Eq. (1) in each slice of thickness h, we can determine the evolution of the internal electric field and, consequently, by way of the Pockels effect, the evolution of the index variation δn in the longitudinal section xz. The next steps are obtained by repeating the process of propagating the same input beam along the new index profile and again solving Eq. (1) in each slice. The gyratory power characteristic of the sillenite family is accounted for in the BPM calculation, this parameter being crucial for self-focusing [18,19]; it is done by considering that $\mathcal{E}$ is a vector field with two complex transverse components.

However, the physical phenomenon is a $(2+1)$-dimensional process (two transverse diffraction directions and one propagation direction). The experimental studies were performed using the measurement method described before: the slit was positioned orthogonally to the applied electric field, thus allowing us to measure the self-focusing phenomenon parallel to it (x direction). This will allow us to compare our measurements to numerical simulations performed by the BPM, although we are aware that our $(1+1)$D model might still be incomplete.

These calculations involve very detailed parameters of the crystal, namely, the donor and acceptor densities, the static dielectric permeability, the photoionization cross section, the carriers mobility, etc. Since the literature does not yield values for all of them in $Bi_{12}TiO_{20}$, we have chosen to use the values given for $Bi_{12}SiO_{20}$ [20–22], which also belongs to the sillenite family, assuming they are close to those of $Bi_{12}TiO_{20}$. For instance, $N_D=10^{19}$ cm^{-3}, $N_A=10^{16}$ cm^{-3}, $\varepsilon=56$ from Ref. [20], and $s=2\times10^{-5}$ $|m^2/J$ from Ref. [22]. As pointed out by Roosen *et al.* [21], there is, however, a slight uncertainty on the value of the carrier mobility μ in the pulsed regime. We have thus chosen to let μ be a free parameter in our simulations, between 3×10^{-2} cm^2/V s and 3 cm^2/V s.

Figure 3 shows four examples of such simulations with four distinct values of μ, namely, 3×10^{-2}, 0.1, 0.3, and 0.5 cm^2/V s, the rest of the parameters being set to those of the experiment described in the previous section. The value of the mobility μ was varied to optimize the fit between the experimental data and the simulated curves. For $\mu=3\times10^{-2}$ cm^2/V s and $\mu=0.1$ cm^2/V s, the diffraction coefficient versus time decreases slightly indicating a small self-focusing effect not as large as the experimental one. Matching theoretical results can be obtained, as shown in Fig. 3, for higher mobility values and especially for the value $\mu=0.5$ cm^2/V s. The shape of the experimental curve is retrieved, in particular in the region of the maximum of the pulse ($t=\tau_p/2=4.5$ ns) with a slight gap between the simulation and the measurements at the beginning of the laser pulse (between 1 and 3 ns). The discrepancy observed at the beginning of the pulse need not be interpreted as a mobility evolution. Indeed, at the pulse beginning, the measurement noise is much larger because the absolute intensity measured is much lower than at the pulse maximum.

Our calculations were also performed as a function of the external applied electric field for the value of the mobility determined in Fig. 3: $\mu=0.5$ cm^2/V s. Figure 4 shows a comparison between the experimental diffraction coefficient and our theoretical predictions, as a function of the applied electric field, both for the pulse mid-point (at $t_N=\tau_p/2$) and at its end (at $t_N=\tau_p$). Both experimental and theoretical curves show a quasilinear behavior of the diffraction coefficient α versus the electric field at the two particular times $t_N=\tau_p/2$ and $t_N=\tau_p$ for electric field values greater than 1 kV/cm: the phenomenon appears for E_{ext} above this value. Figure 4 show that good agreement is also retrieved for the value of the mobility found theoretically for different applied electric fields: the theoretical curve is within the error margin of the experimental one.

IV. CONCLUSION

In summary, we have demonstrated experimentally and theoretically that a single 5 ns laser pulse can be self-focused in a photorefractive medium, namely, a $Bi_{12}TiO_{20}$ sample in our case. Furthermore, a simple one-donor-level band transport model introduced in a BPM calculation describes correctly the behavior of the self-focusing observed, both versus time and versus the applied electric field.

ACKNOWLEDGMENTS

The authors would like to thank Dr. D. Rytz, from the Forschunginstitut für mineralishe und metallische Werkstoffe Edelsteine/Edelmetalle (Idar-Oberstein, Germany) for useful discussions and for his BTO crystal on which our experiments were conducted. The theoretical considerations of this paper, involving highly intensive computation, were developed with the support of the Centre Charles Hermite (Nancy, France), on their 64 processor Origin 2000. This work was supported in part by the Region Lorraine.

[1] M. Segev, B. Crosignani, and A. Yariv, Phys. Rev. Lett. **68**, 923 (1992).
[2] M. Castillo *et al.*, Appl. Phys. Lett. **64**, 408 (1994).
[3] M. Segev, Y. Ophir, and B. Fischer, Appl. Phys. Lett. **56**, 1086 (1990).
[4] B. Crosignani *et al.*, J. Opt. Soc. Am. B **10**, 443 (1993).
[5] G. C. Duree *et al.*, Phys. Rev. Lett. **71**, 533 (1993).
[6] S. R. Singh and D. N. Christodoulides, Opt. Commun. **118**, 569 (1995).
[7] A. A. Zozulya and D. Z. Anderson, Phys. Rev. A **51**, 1520 (1995).
[8] G. C. Valley *et al.*, Phys. Rev. A **50**, 4457 (1994).
[9] A. A. Zozulya and D. Z. Anderson, Opt. Lett. **20**, 837 (1995).
[10] N. Fressengeas, J. Maufoy, and G. Kugel, Phys. Rev. E **54**, 6866 (1996).
[11] N. Fressengeas, D. Wolfersberger, J. Maufoy, and G. Kugel, J. Appl. Phys. **85**, 2062 (1999).
[12] N. Fressengeas, D. Wolfersberger, J. Maufoy, and G. Kugel, Opt. Commun. **145**, 393 (1998).
[13] K. Kos, G. Salamo, and M. Segev, Opt. Lett. **23**, 1001 (1998).
[14] M. Segev, M. Shih, and G. C. Valley, J. Opt. Soc. Am. B **13**, 706 (1996).
[15] P. Aguilar, J. S. Mandragon, S. Stepanov, and V. Vysloukh, Phys. Rev. A **54**, 2563 (1996).
[16] G. Quirino *et al.*, Opt. Commun. **123**, 597 (1996).
[17] N. V. Kukhtarev *et al.*, Ferroelectrics **22**, 949 (1979).
[18] S. R. Singh and D. Christodoulides, J. Opt. Soc. Am. B **13**, 179 (1996).
[19] W. Krò̀likowski, N. Akhmediev, D. R. Andersen, and B. Luther-Davies, Opt. Commun. **132**, 179 (1996).
[20] G. LeSaux, G. Roosen, and A. Brun, Opt. Commun. **56**, 374 (1986).
[21] G. Roosen *et al.*, Rev. Phys. Appl. **22**, 1253 (1987).
[22] D. C. Jones and L. Solymar, Opt. Commun. **85**, 372 (1991).